Structure–property–function relationships of supercritical CO2-processed amniotic membrane: An ex vivo ocular proof of concept

L. Adam, Solène Rota, Flora Lemaire, Christine Guillaume, Nicole Bouland, Alexis Da Rocha, Adrien Baldit, Quentin C.P. Bourgogne, Jennifer Rodon Fores, Fabienne Quilès, et al.

Materials & Design 265 (2026) 115964

Contents lists available at ScienceDirect

Materials & Design

journal homepage: www.elsevier.com/locate/matdes

Structure–property–function relationships of supercritical CO_2-processed amniotic membrane: An ex vivo ocular proof of concept

L. Adam [a,b], S. Rota [b], F. Lemaire [a], C. Guillaume [a], N. Bouland [c], A. Da Rocha [d,e], A. Baldit [d], Q. Bourgogne [d], J. Rodon-Fores [f], F. Quilès [g], C. Mauprivez [a], R. Bardonnet [b], H. Kerdjoudj [a,*]

[a] Université de Reims Champagne Ardennes, UR 4691 BIOS, Reims, France
[b] BIOBank, France
[c] University de Reims Champagne Ardennes, URCATECH, Reims, France
[d] Université de Lorraine, CNRS, Arts et Métiers ParisTech, LEM3, F-57000 Metz, France
[e] Université de Strasbourg, CNRS, ICube UMR 7357, 67000 Strasbourg, France
[f] Université de Strasbourg, CNRS Institut Charles Sadron, Strasbourg, France
[g] Université de Lorraine, CNRS, LCPME, F-54000 Nancy, France

ARTICLE INFO

Keywords:
Supercritical carbon dioxide
Sterilization
Amniotic membrane
Biocompatibility
Ocular repair

ABSTRACT

Human amniotic membrane (AM) exhibits a range of biological and structural properties that support its clinical use in regenerative medicine, particularly for ophthalmologic applications. This study aims to develop a readily available, sterile AM using modified (m)-Supercrit® process. Compared with freeze-drying, m-Supercrit® processing produces a transparent, thin, and hydrophilic membrane, key attributes for corneal applications. Mechanistically, m-Supercrit® processing induces marked alterations in collagen and glycosaminoglycan composition, which are associated with a significant increase in the membrane's linear elastic modulus. Although m-Supercrit®-processed AM shows a reduction in bioactivity and cell migration, including a significant decrease in HGF and b-FGF levels, it retains essential biological functions such as hemocompatibility, cytocompatibility, cell adhesion/proliferation, anti-inflammatory, and anticancer activities. Importantly, the clinical feasibility of handling and suturing m-Supercrit®-processed AM is demonstrated in an *ex vivo* ocular surface model. Overall, these findings support the m-Supercrit® process as a promising strategy for developing an off-the-shelf, sterile amniotic membrane suitable for ophthalmologic clinical applications.

1. Introduction

Temporary biological coverage using allografts and xenografts is often used to improve tissue healing. Amniotic membrane (AM) was first used by Davis in 1910 for skin transplantation,[1] then by de Rotth for ocular surface reconstruction.[2] AM is readily accessible and ethically uncontroversial. It is routinely discarded following deliveries and can be collected under standardized, sterile conditions with informed consent. This makes it an attractive, low-cost, and sustainable source of biological coverage. Possession of clinically important characteristics, including low immunogenicity and anti-inflammatory, anti-fibrotic, anti-angiogenic and anti-microbial properties, have made AM a potential candidate for several applications such as membrane mucous pemphigoid and Stevens–Johnson syndrome, pterygium, persistent epithelial defects with ulceration, conjunctival surface reconstruction and ocular surface reconstruction in patients with chemical and thermal burns,[3] attesting to their safety and translational viability. Although the clinical application of AM is considered safe, complications have been reported. In particular, the risk of transmitting pathogens to recipients is possible especially if it is not processed using aseptic techniques or if storage conditions are improper. Although AM can be used in a "fresh" state, in most countries, because of their legal regulation, AM must be preserved for six months until confirming biological safety (*i.e.*, a negative screening result for HIV, VHB, VHC).[4] To date, several basic preservation methods for storing AM have been developed, such as cryopreservation, lyophilization, and air drying.[5] Each of these methods remarkably affects the mechanical, physico-chemical, and biological properties of AM. Antibiotic–antimycotic cocktail is commonly used for

* Corresponding author at: Université de Reims Champagne Ardenne, 1 avenue du Maréchal Juin, 51100 Reims, France.
E-mail address: halima.kerdjoudj@univ-reims.fr (H. Kerdjoudj).

https://doi.org/10.1016/j.matdes.2026.115964
Received 11 February 2026; Received in revised form 23 March 2026; Accepted 1 April 2026
Available online 5 April 2026

AM decontamination, which are not sufficient for sterility assurance.[6] Consequently, the AM sterilization by physical or chemical methods is needed. Gamma irradiation and peracetic acid/ethanol mixtures are commonly used for the terminal sterilization of freeze- or air-dried AM; however, these methods may induce structural alterations in the extracellular matrix (ECM) and exhibit limited penetration within the tissue.[7] Supercritical carbon dioxide ($scCO_2$) is a promising method for terminal sterilisation due to its high penetrative capacity. Above its critical temperature (31.1°C) and critical pressure (73.9 bar), CO_2 behaves as a supercritical fluid with low viscosity, high diffusivity and liquid-like density, allowing efficient penetration into microporous structures such as dense tissues.[8] In addition, CO_2 is non-toxic, non-flammable, inexpensive, and leaves no residue after depressurization, making it an environmentally friendly solvent. However, $scCO_2$ alone is generally insufficient to achieve complete sterilization of biological tissues. Therefore, it is often combined with additives such as peracetic acid and ethanol, which enhance sterilization efficiency by improving penetration into tissue microstructures, without inducing toxicity.[9] A limited number of studies have reported successful sterilization of AMs using $scCO_2$ while preserving structural integrity and key ECM components.[10] Here, we present a two-part study: first, examining the sterility assurance level of scCO2-processed AM (modified-Supercrit® (m-Supercrit®) process; BIOBank, PCT/FR2023/051010) according to the European Pharmacopoeia. We further compared the structural, mechanical, and functional properties of scCO2-processed AM with freeze-dried AM.

2. Material and methods

2.1. Preparation of samples and characterization

Human placentas (n = 10), obtained from the Reims maternity hospital, Champagne-Alix, were transferred in a Class II biological safety cabinet, and the fetal chorioamniotic tissues of each placenta were manually peeled in sterile conditions. The peeled membranes were washed in PBS to remove debris, blood, and remnants of amniotic fluid. The chorion was carefully separated from the amniotic membrane (AM).[11] Isolated AM were rinsed in PBS and then deposited onto polyethylene mesh carrier (Sefar medifab petex), with epithelial side up,[4] placed in two Tyvek® packages, heat-sealed, and stored at − 20°C prior to shipment to BIOBank. Carriers help to recognize side-orientation.

2.2. m-Supercrit® processing

The process involved circulating supercritical carbon dioxide ($scCO_2$) at 140 bar and 40°C, according to Supercrit® patent pending process (BIOBank, PCT/FR2023/051010) [SR1]. Briefly, a solution of hydrogen peroxide (H_2O_2, 3% *v/v* in ethanol 10%) was injected in the $scCO_2$ stream for 50 min at a rate of 1 mL/min, acting as a co-solvent to the $scCO_2$. After a time contact with samples for 3 h, dissolved H_2O_2 was separated from the $scCO_2$ while the latter continued to circulate. A solution of peracetic acid (PAA, 4% *v/v* in ethanol 99%) was then injected, applied and separated under the same operating conditions as the H_2O_2 solution. Following this treatment, samples were subsequently rinsed twice with 80 mL of ethanol 99% injected in the $scCO_2$ stream at 2 mL/min rate for 40 min. After an overnight drying in $scCO_2$ followed by depressurization of the system, AM $scCO_2$ samples were collected and stored at –20°C. Freeze-dried (FD) AM stored at − 20°C were used as control.

2.3. Thermogravimetric analysis (TGA)

Thermal degradation was analysed using TGA with a SDT650 from TA Instrument™. To unsure the repeatability of the results, the weight of the samples was controlled before the tests. AM_{scCO2} and AM_{FD} samples (n = 2) were analysed with TGA by a continuous heating to 600°C at 5°C/min, allowing both the quantification of water absorption and the sample composition. All of tests were conducted at a pressure of 1.5 bar of air. Preliminary tests on these samples showed an experimental error of ± 0.7%.

2.4. Scanning electron microscopy (SEM)

Samples (n = 4) were cryo-fractured in cross-section using liquid nitrogen and sputter-coated with a thin gold–palladium layer (JEOL JFC-1100, France). Samples were then observed and the thickness was determined using a SEM (EVO 10, Zeiss, Germany).

2.5. Transmittance

The absorbance (A) of AM_{FD} and AM_{scCO2} samples (n = 4) in dried and hydrated state was measured using a FLUOstar Omega microplate reader (BMG Labtech, France). Samples were placed in 96-well plates, and A was recorded at 300 nm to 650 nm. Transmittance was calculated using the following equation:

$$\text{Transmittance}\ (\%) = 10^{2\text{-}A}$$

2.6. Swelling capacity

Samples (10 mg; n = 4) were immersed in distilled water for 15 min and weighed (M). Rehydration capacity was calculated using the following equation:

$$\text{Swelling capacity}\ (\%) = \frac{M - 10}{10} \times 100$$

2.7. Total porosity

Samples (10 mg; n = 4) were immersed in absolute ethanol for 15 min and weighed (M). Total porosity, defined as the pore volume occupied by ethanol, was calculated using the following equation:

$$\text{Porosity}\ (\%) = \frac{M - 10}{M} \times 100$$

2.8. Wettability

A drop of distilled water (5 µL) was deposited onto the surface (*i.e.* amniotic and chorionic sides) of samples (n = 4) using a microsyringe. The contact angle was immediately captured using a goniometer (KRÜSS, DSA25, Germany) equipped with a camera perpendicular to the surface. The angles were measured to the left and right of the droplet, and the average of the two values was automatically calculated.

2.9. Infrared (IR)

IR spectra, in transmission mode, were recorded between 4000 and 800 cm^{-1} on a Bruker Vertex 70v spectrometer controlled by OPUS 7.5 software, and equipped with a Hyperion 2000 microscope and a (×15) objective. A KBr beam splitter and a MCT detector were used. The resolution of the single beam spectra was 4 cm^{-1}. Masks of 400 µm × 400 µm were used to record at least three spectra at different areas of the analyzed membrane. The number of bidirectional double-sided interferogram scans was 64, which corresponds to a 40 s accumulation. All interferograms were Fourier processed using the Power phase correction mode and a Blackman-Harris 3-term apodization function. Measurements were performed at 21 ± 1°C in an air-conditioned room. Water vapor subtraction was performed when necessary, and baseline was corrected at 3800, 2500, 1900 and 900 cm^{-1} before further analysis.

2.10. Arachidonic acid (AA)

The content in AA was determined using Arachidonic acid™ Assay

kit (Aviva System Biology, USA). Briefly, samples (n = 4) were washed in PBS, sonicated twice for 20 min at 37°C and centrifuged at 10000*g* for 10 min. The as-supernatants were collected and stored at 4°C until use. 50 μL of supernatant and standards were added to the plate and incubated with the biotin-labeled antibody solution for 45 min at 37°C. The plate was then incubated with the HRP–streptavidin conjugate for 30 min at 37°C, followed by incubation with 3,3′, 5,5″-tetramethylbenzidine substrate solution for 20 min at 37°C in the dark. For each step, the plate was washed three times with wash-Buffer solution. The reaction was stopped, and A was measured at 570 nm. AA concentrations were calculated using the following equation:

$$[\mathrm{AA\,(mg/mL/g)}] = \frac{A_E}{a}$$

where A_E is the absorbance of AM_{FD} and AM_{scCO2} samples and (a) is the slope of the standard curve.

2.11. DNA quantification and nuclear staining

DNA was extracted from samples (n = 4) using the MasterPure™ DNA Purification Kit (Epicentre® Biotechnologies, France). According to the manufacturer's instructions, the extracted DNA was quantified using the Quant-iT™ PicoGreen™ dsDNA kit (ThermoFisher Scientific, France). Briefly, 100 μL of samples and standards were added to the plate and incubated with the Quant-iT™ PicoGreen™ dsDNA reagent for 5 min at room temperature. Fluorescence was measured at 450/520 nm. Cell nuclei were stained with diamidino-4′,6-phénylindol-2 dichlorhydrate (DAPI, 100 ng/mL, 1:1000 dilution in distilled water) for 15 min. After two washes in PBS for 5 min, samples were observed using an epifluorescence microscope (Axiovert 200 M, Zeiss, Germany, Objective × 10).

2.12. Histology

Samples were fixed in 4% (*v/v*) formaldehyde (Sigma-Aldrich, France) at room temperature for 48 h. Samples were dehydrated overnight through graded ethanol solutions and cleared in xylene baths. The samples were embedded in molten paraffin, and 3 μm-thick sections were cut using a rotary microtome (RM2055, Leica Microsystems, France). Sections were mounted onto glass slides and incubated overnight at 42°C. After deparaffinization in xylene, sections were rehydrated in distilled water for 5 min and stained with Hematoxylin–Eosin–Saffron, Masson's trichrome, Alcian blue at pH 1.5 and 2.5, according to the manufacturers' instructions. Slides were scanned (120 OLYMPUS scanner) and analyzed using QuPath® software.

2.13. Second harmonic generation (SHG)

Samples were imaged using two-photon excitation laser scanning confocal microscopy with Single-scan polarization-resolved SHG (CLSM 710-NLO, Carl Zeiss SAS, Germany), coupled to a Chameleon femtosecond titanium–sapphire laser.

2.14. Collagen, sulfated glycosaminoglycan (GAGs) and hyaluronic acid (HA)

Samples (3 mg; n = 4) were ground using a metal ball mill (Precellys®, Bertin Technologies) before processing. Collagen was quantified using the Sircol™ Insoluble Collagen Assay kit (Biocolor, UK). According to the manufacturer's protocol, samples were incubated overnight at 4°C in a pepsin solution (3 mg/mL in 0.1 M acetic acid) and centrifuged at 10000*g* for 10 min. 100 μL of supernatants and standards curve were mixed with Sircol dye reagent and incubated at 25°C for 30 min. Samples were centrifuged at 250*g* for 10 min, washed with acid–salt wash reagent to remove unbound dye, and centrifuged again. Pellets were resuspended in alkali reagent, and A was measured at 550 nm. GAGs content was determined using the Blyscan™GAG Assay kit (Biocolor, UK). Briefly, samples were incubated overnight at 65°C in 1 mL of papain solution (Calbiochem) and centrifuged at 10000*g* for 10 min. 100 μL of supernatants and standards curve were mixed with Blyscan dye reagent for 30 min, followed by centrifugation at 250*g* for 10 min. Pellets were resuspended in dissociation reagent, and A was measured at 550 nm. HA content was measured using a Hyaluronan™ Assay kit (Biocolor, UK). Samples were incubated overnight at 65°C in 1 mL of proteinase K solution (1:20 dilution in Tris–HCl) and centrifuged at 10000*g* for 10 min. 100 μL of supernatants and standards curve were incubated with a GAG precipitation reagent for 15 min and centrifuged at 250*g* for 10 min. Pellets were resuspended in distilled water, and HA was precipitated using cetylpyridinium chloride. Pellets were washed with 98% (*v/v*) ethanol, resuspended in distilled water, stained with Dye Reagent (20 μL), and A was measured at 655 nm. Collagen, GAG and HA contents were calculated using the following equation:

$$[\mathrm{Concentration}] = \frac{A_E}{a}$$

where A_E is the absorbance of samples and (a) is the slope of the corresponding standard curve.

2.15. Circular dichroism (CD)

CD was performed using four-times diluted digest solutions (10 mg/mL in 0.1 M acetic acid) placed in a 0.1 mm path quartz cuvette. Spectra were recorded on a CD spectrophotometer J1700 (Jasco, France) between 190 and 250 nm. The data pitch was 0.5 nm, CD scale 20mdeg, D.I.T. 2 s, and bandwidth 1.0 nm. Five accumulations were made for each spectrum at a rate of 20 nm/min.

2.16. Mechanical properties

Samples (n = 6) were tested by quasi-static tensile tests until failure as previously described.[12] A Zwicky Universal Testing Machine (Zwick Roell, Germany) equipped with a 10 N load cell was used to measure the response of the samples. The loading sequence was divided into two stages: a dry test under the linear elastic limits with an imposed deformation of around 1.8%, avoiding the tissue damage, followed by a hydrated test (NaCl 0.9%, *w/v, 37°C*), allowing a characterization of the mechanical response. Between the two steps, the sample was given 5 min to hydrate and reach osmotic balance before being tested with 1.6% strain loads at a speed of 0.01 mm/s to stay within the quasi-static frame. The engineer definition of stress and strain was used to process the force–displacement curves and determine the linear elastic moduli.

2.17. Biocompatibility

Human foreskin and blood were obtained from Pediatric Surgery Department, American Hospital, CHU of Reims and Etablissement Français du sang, respectively. AM samples were punched (8 mm in diameter) and decontaminated by UV exposure (30 min) before use.

2.18. Hemolysis index

Samples (n = 4) were incubated in 24-well plates with 200 μL of whole human blood and 1.8 mL of PBS. After 4 h of incubation at room temperature, 200 μL of supernatant were transferred to a 96-well plate, and A was measured at 540 nm. The hemolysis index was calculated using the following equation:

$$\mathrm{Hemolysis\,index} = \frac{(A_S - A_N)}{(A_P - A_{N)}} \times 100$$

where A_S, A_P, and A_N correspond to the absorbance of hemoglobin in the presence of samples, distilled water (positive control), and PBS (negative control), respectively.

2.19. Cytocompatibility

Foreskin-derived fibroblasts (FDs; n = 6) were extracted by separating dermis epidermis, mincing into ~ 1 mm^2 fragments, and culturing in T12.5 flasks with DMEM supplemented with 10% FBS and 1% PSA at 37°C and 5% CO_2. At 80% confluence, cells were trypsinized and expanded until second passage.

2.20. Cytotoxicity

DFs were seeded to each 24 well at 10^4cells/ well with DMEM supplemented with 10% FBS and 1% PSA. DFs were incubated at 37°C with 5% CO_2 until reaching 80% of confluence. Samples (n = 4) were added to the well and incubated for 24 h. DFs cultured without samples were used as control. The evaluation of the DFs metabolic activity was carried out by a water-soluble tetrazolium salt (WST-1®, 1:10 in DMEM without phenol red) assay (Roche Diagnostics, France). According to the manufacturer's protocol, A was measured at 440 nm with a correction at 750 nm, using a FLUOstar Omega microplate reader.

2.21. Cell proliferation and morphology

Samples (n = 4) were placed in 48-well plates and seeded with DFs at a density of 2 × 10^4 cells/cm^2. After 4, 7, and 10 days of culture, cells were washed with 1 × PBS and their metabolic activity was assessed using the WST-1® as described above. After 10 days of culture, cells were fixed in paraformaldehyde, and F-actin labelling was performed using with Alexa Fluor® 488–conjugated phalloidin (1:100 dilution in 0.5% BSA; Invitrogen) and visualized by CLSM 710-NLO. Samples were also fixed with glutaraldehyde for 1 h then rinsed twice with distilled water for 10 min, dehydrated through graded ethanol solutions, and dried using hexamethyldisilazane for 24 h. After gold–palladium coating, samples were observed by SEM.

2.22. Bioactivity

Samples (n = 4) were weighed and 10 mg of each were incubated in 1 mL of DMEM supplemented with 1% PSA for 48 h and centrifuged at 10000*g* for 10 min. The resulting conditioned media was kept at −20°C until use.

2.23. Growth factor release

The released growth factors from AM samples was quantified, using ELISA kits, including Human DuoSet® VEGF, HGF, FGF-b, IGF, and TGF-β (R&D Systems), according to the manufacturer's protocols.

2.24. Incucyte® migration assay

Wound healing assay was performed on DFs that were seeded at 4 × 10^4cells/well in 96-well plates in DMEM supplemented with 20% FBS and 1% PSA. A day after, a scratch wound was generated using the IncuCyte® WoundMaker instrument. Non-adherent cells were removed by two washes with PBS, FDs were cultured in the presence of conditioned media. DFs cultured in DMEM supplemented with 10% FBS were used as positive control. Images were recorded every 4 h for 48 h using the Incucyte ZOOM live-cell analysis system. Wound area was quantified and expressed as the percentage of wound closure (Incucyte® software).

2.25. Anti-cancer viability

MDA-MB231 cell line at a density of 1 × 10^4cells/cm^2 were cultured in the presence of samples for 24 and 72 h. Cell metabolic activity was assessed using the WST®-1 assay as described above.

2.26. Neutrophil (PNNs) activation

Human PNNs were isolated from human peripheral blood (n = 6) with Polymorphprep® (ProteoGenix, France). PNNs were seeded to each 24 well at 10^6cells/ well and incubated at 37°C and 5% CO_2 in the presence of RPMI-Glutamax® (Gibco), autologous serum (2.5%, *v/v*) and PSA 1%, with or without lipopolysaccharide and samples (LPS, 10 ng/mL, Sigma Aldrich). After 2 h of contact with samples, PNNs were washed in PBS and intracellular ROS were labeled using Muse® Oxidative Stress Kit (Luminex, USA) and analyzed by flow cytometry with the LSRFortessaTM system (BD Biosciences). Released IL-8 was quantified using an IL-8 DuoSet® ELISA kit (R&D Systems), following the manufacturer's instructions.

2.27. Macrophage activation

U937 cell line (n = 3) was differentiated in M0 as previously described.[13] 10^6cells were seeded in 12-well plate and cultured in the presence of RPMI-Glutamax® supplemented with FBS (0.5%, *v/v*), PSA (1%, *v/v*), phorbol 12-myristate 13-acetate (PMA, 25 nM, ThermoFisher) and Vitamin D3 (20 nM, Sigma Aldrich) overnight. Media were refreshed by RPMI-Glutamax® with FBS (5%, *v/v*), PSA (1%), PMA (25 nM) and Vitamin D3 (20 nM) and incubated for 24 h at 37°C. Macrophages were cultured for 48 h at 37°C in PMA free medium mix then samples were added and cultured for 48 h at 37°C and 5% CO_2. Culture media were collected and stored at − 20°C until analysis. The release of the pro-inflammatory cytokine TNF-α and IL-10 was quantified using DuoSet® ELISA kits (R&D Systems).

2.28. Going further ocular application

Circular AM samples with a diameter of 16 mm^2 were sutured onto the ocular surface (porcine eyes, local slaughterhouse) by placing nine evenly distributed sutures around the perimeter of the sample. Sutures were performed on the sclera, close to the limbal region, using surgical sutures (thread size: 10–0). Following suturing, the eyes were fixed in 4% formaldehyde. After fixation, samples were dehydrated and embedded in paraffin. Histological sections of 5 μm-thickness were then prepared and stained with Masson's trichrome and slides were scanned (120 OLYMPUS scanner) and analyzed using QuPath® software.

2.29. Statistical analysis

Structural analyses were conducted on four samples per condition. Hemolysis assays were conducted on four samples per condition using blood from three donors. Biological tests were performed in triplicate per condition using cells from six donors. Tests involving MDA-MB-231 were used in triplicate. All data were analyzed using GraphPad Prism 10. Graphs and statistical analyses were performed using the Mann–Whitney non-parametric test or *t*-test. A p-value < 0.05 was considered statistically significant.

2.30. Ethical statement

All human samples including placenta, foreskin and blood used in this study were obtained from informed patients with written consent and in accordance with legal and ethical guidelines (Article R 1243–47). All procedures were conducted with the appropriate authorization and registration number (DC-2014—2262) issued by the French National "Cellule de Bioethique".

3. Results and discussion

While numerous clinical studies clearly demonstrated the wound-healing properties of the amniotic membrane (AM), significant challenges remain regarding its processing and storage at room temperature for commercially available products.[14] Indeed, the requirement for sterile storage at low temperatures limits the shelf life of AM, rendering it unsuitable as a readily deployable therapy for military applications or for use in developing countries, where maintaining a cold chain is logistically challenging. Supercritical carbon dioxide ($_{SC}CO_2$) sterilization is an emerging technology for the processing of biological tissues.[9] Although CO_2 in its supercritical state provides relatively mild sterilization conditions, its antimicrobial efficacy is significantly enhanced by the addition of agents such as peracetic acid (PAA), which induce oxidative damage to microbial components, including membrane lipids, proteins, and DNA, ultimately leading to cell inactivation.[15] An outstanding advantage of PAA is its low toxicity, as its residues (*i.e.*, O_2, CO_2, and H_2O) are natural and harmless.

3.1. Sterile state of m-Supercrit® processed-AM

AM can be contaminated by normal vaginal flora; however, the risk of contamination can be minimized by sterilising the AM using $_{SC}CO_2$. This study demonstrates that an appropriate sterility assurance level (SAL) of AM is achieved using m-Supercrit® process (BIOBank, PCT/FR2023/051010). The accepted sterility threshold is a SAL of 10^{-6}.[16] Sterility was assessed in accordance with the European Pharmacopeia sterility test guidelines. The m-Supercrit® process, applied to packed and based on $_{SC}CO_2$ sterilization (AM_{scCO2}), results in a negative bacterial culture, with no detectable colony forming unit on agar. In contrast, freeze-dried AM (AM_{FD}) exhibits a positive bacterial culture ($8.3 \times 10^6 \pm 3.2 \times 10^6$CFU/mL; Fig. SI-1). To sum up, the effectiveness of the sterilization using m-Supercrit® process was achieved by adding H_2O_2 (~300 ppm), PAA (~400 ppm) and ethanol (~15000 ppm) while the time of circulation was based on a preliminary optimization study. Based on these results, the structural and biological performance of AM_{scCO2} was further evaluated. AM_{FD} was used as control.

3.2. Thermal stability and structural features of m-Supercrit® processed-AM

Reducing water availability is advantageous for controlling allograft deterioration, as it inhibits microbial growth and extends product shelf life.[17] As $scCO_2$ is known to be an effective drying technique[18] thermogravimetric analysis (TGA) was performed on AM_{scCO2} to determine the residual moisture and the thermal stability of the organic component (Fig. 1A). Since TGA measures both surface and bound water, the residual water content of the AM_{scCO2} sample estimated from the weight loss after AM heating at 130°C is ~ 12%. This value is comparable to that of AM_{FD} and is close to the 10% residual moisture threshold established by the European Directorate for the Quality of Medicines & HealthCare for biological membranes, including AM and cornea.[19] The TGA curves also reveal a pronounced thermal degradation and significant mass loss occurring in the temperature range of

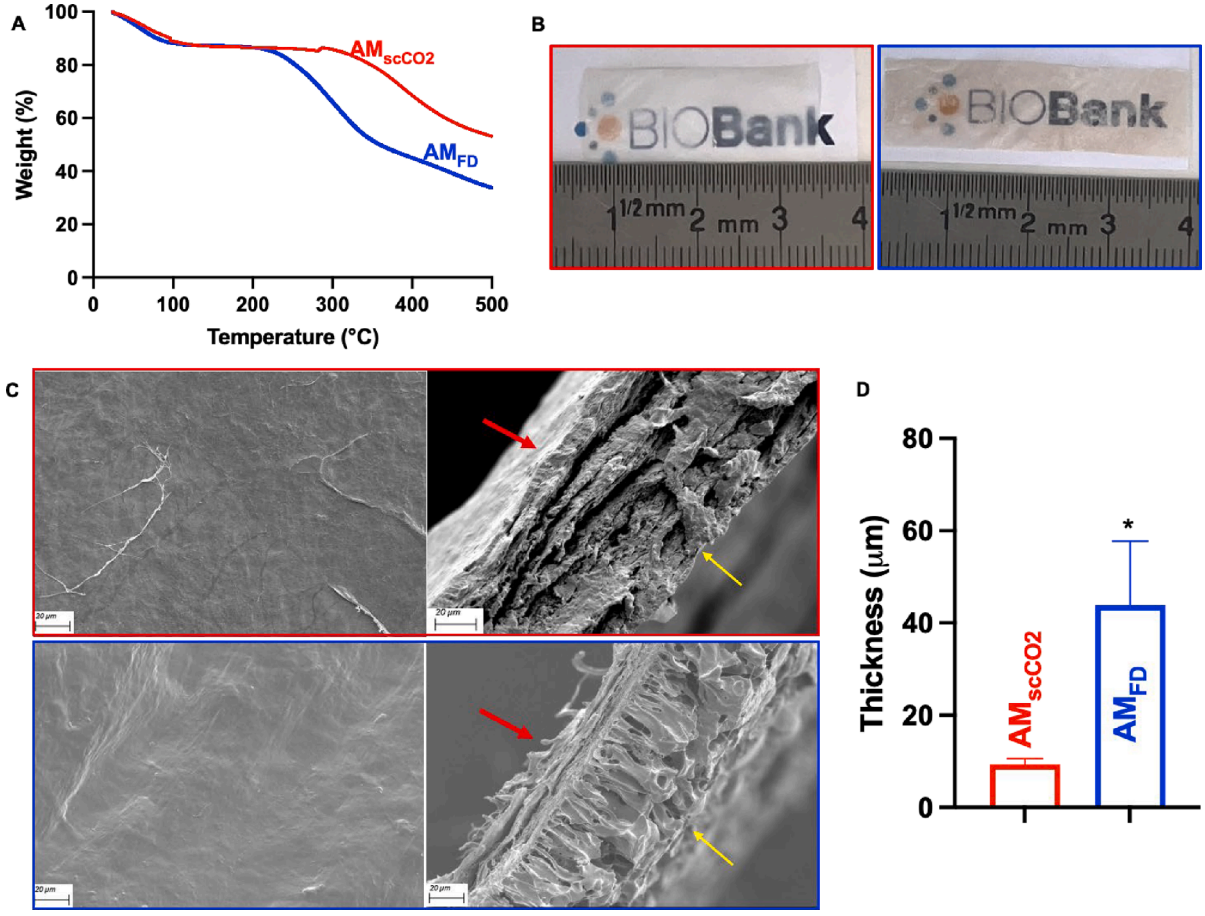

Fig. 1. Thermal and structural characterization of m-Supercrit® processed amniotic membrane (AM_{scCO2}; highlighted in red) and freeze-dried amniotic membrane (AM_{FD}; highlighted in blue). A: TGA (A), macroscopical views (B) and SEM images on the surface (left column) and section (right column) (C) of dried AM samples. Red arrows indicate amniotic side and yellow arrows indicate chorion side. Scale bars = 20 µm. Histograms showing the thickness of the dried membranes (D; (*)$p < 0.02$, Mann Whitney test, n = 4). (For interpretation of the references to colour in this figure legend, the reader is referred to the web version of this article.)

300 − 500°C, a signature of collagen degradation.[20] At 500°C, the mass loss is 39% for AM_{scCO2} compared with 33% for AM_{FD}. The temperature corresponding to 50% mass loss ($T°_{50}$) increases from 353°C for AM_{FD} to 395°C for AM_{scCO2}. Taken together, these findings demonstrate that AM_{scCO2} has higher thermal stability than AM_{FD}.

Transparency of AM is important for the ophthalmic usage and corneal reconstruction purposes. The macroscopic and microscopic appearance of the AM_{scCO2} and AM_{FD} are presented in Fig. 1B-1C. Macroscopical visualization doesn't reveal any obvious differences between the two dehydrated samples. The very low transmittance of the dehydrated samples (*i.e.*, average transmittance at 650 nm < 2%) is likely attributable to the reduced inter-fiber spacing within the ECM, which limits light transmission by increasing irregular light scattering and thereby reducing membrane transparency. Scanning electron microscopy (SEM) reveals the presence of the two characteristic sides of the AM: the smooth amnion side, rich in epithelial cells, and the spongy chorion side.[21] However, slight ultrastructural modifications are observed in AM_{scCO2} which exhibits a marked reduction in spongy-layer thickness compared to AM_{FD} (10.5 ± 0.8 μm for AM_{scCO2} *vs.* 30.1 ± 2.66 μm for AM_{FD}, $p < 0.02$, Mann-Whitney, Fig. 1D) along with a more compressed wall structure and smaller pores.

When hydrated AM_{scCO2} was placed over a cardboard support, the "BIOBank" text printed on the cardboard is clearly visible, indicating a high level of transparency (Fig. 2A). Quantitative light transmission measurements show that the average transmittance of AM_{scCO2} exceeds 82 ± 5%, compared with 72 ± 8% for AM_{FD} ($p < 0.01$, Mann-Whitney, Fig. 2B). To determine the amount of AM_{scCO2} required to absorb the fluids, porosity, swelling behaviour, and surface wettability were assessed. AM_{scCO2} is highly swellable [22] since it exhibits an equilibrium water content of 1077 ± 35%, while AM_{FD} shows a comparable value of 1093 ± 33% (Fig. 2C). Liquid displacement analysis reveals a total porosity of 90 ± 1.3% for AM_{scCO2} and 88 ± 1.9% for AM_{FD} (Fig. 2D). Contact angle measurements performed on both sides indicate a hydrophilic epithelial layer (<45°) and a more hydrophobic spongy layer (>45°, Fig. 2E). While no change is observed for the epithelial side, the spongy side showed a significant decrease in contact angle from 54 ± 6 for AM_{FD} to 49 ± 3 for AM_{scCO2}; ($p < 0.01$, Mann-Whitney, Fig. 2F), suggesting modifications in the physicochemical properties of the spongy-*like* ECM following m-Supercrit® processing.

Preservation of ECM integrity after m-Supercrit® processing is a central objective of this study. In this context, previous reports have shown that $scCO_2$ sterilization has minimal effects on key AM-derived ECM components.[10] The chemical composition of AM_{scCO2} was investigated by infrared (IR) micro-spectroscopy in transmission mode. The band assignments (Table 1) were made using second-derivative spectra and are consistent with the literature.[12] Compared with AM_{FD}, AM_{scCO2} spectra exhibit a pronounced reduction in bands at 2920, 2852 and 1741 cm^{-1}, assigned to long chain CH_2 vibrations and C=O groups originating from cellular phospholipids (Fig. 3A). This observation indicates partial removal of cellular components. Supercritical CO_2 is known for its excellent solvent properties for extracting non-polar compounds.[23] Moreover, the addition of polar cosolvent as ethanol can modulate $scCO_2$ polarity, facilitating the extraction of charged phospholipids molecules. Arachidonic acid, a polyunsaturated fatty acid present in membrane phospholipids, is significantly reduced in AM_{scCO2} (0.46 ± 0.18 mg/mg of dry tissue) compared with AM_{FD} (1.26 ± 0.18 mg/mg of dry tissue, $p < 0.02$, Mann-Whitney; Fig. 3B), supporting tissue decellularization hypothesis. Exposure to $scCO_2$ has previously been reported as a physical decellularization method for biological tissues.[24] According to Crapo *et al.*, a tissue is considered as decellularized when the residual double-stranded DNA (dsDNA) is below 50 ng of per mg of dry mass of tissue.[25] In the study, extracted dsDNA is 68 ± 12 ng/mg for dry mass of AM_{scCO2} *vs.* 104 ± 11 ng/mg of dry mass AM_{FD} ($p < 0.02$, Mann-Whitney, Fig. 3C). Despite the significant decrease in dsDNA, these values don't meet the acceptance decellularization threshold. Furthermore, nuclei are still clearly visible in DAPI stained samples and hematoxylin-eosin-safran stained histological sections (Fig. 3D-E). Furthermore, AM_{scCO2} exhibits better preserved

Table 1
Infrared micro-spectroscopy: Assignments of principal infrared vibrational bands of amniotic membrane samples.

Wavenumber (cm^{-1}) AM_{scCO2}	AM_{FD}	Assignment
~3440	~3430	νOH
3305	3303	Amide A (proteins)
3202	3205	Amide B (proteins)
3075	3068	νCH aromatic (proteins)
2961	2960	νCH_n
2924	2920	νaCH_2
2875	2875	νsCH_n
2852	2851	νsCH_2
1738	1741	νC=O (esters from PL)
1694	1691	Amide I (collagen)
1659	1655	Amide I, (COL, random/α-helix from proteins)
1632	1634	Amide I (β-sheet, proteins)
1571 (sh)	1568 (sh)	Amide II (COL)
1550	1549	Amide II (random/ α-helix, proteins)
1514	1514	Amide II (β-sheets, proteins)
1465	1465 (sh)	δCH_n
1454	1454	δCH_2
1404	1402	$\nu sCOO^-$ (proteins, GAGs)
1380	1381	δCH_n
1340	1340	Amide III (COL)
1284	1284	Amide III (COL)
1238	1236	νC-N (COL), νaPO_2 (NA, PL) νaSO_2 (GAGs)
1203	1202	dCNH (collagen)
1162, 1130, 1081, 1036, 970	1160, 1115, 1080, 1058, 1032, 971	νC-O, νC-C, νC-O-C (carbohydrate moieties) νsPO_2 (NA, PL), νsSO_2 (GAGs)

Abbreviations: AM_{scCO2}: m-Supercrit® processed amniotic membrane, AM_{FD}: Freeze-dried amniotic membrane, COL: collagen, GAGs: Glycosaminoglycan, NA: nucleic acids, PL: phospholipids.

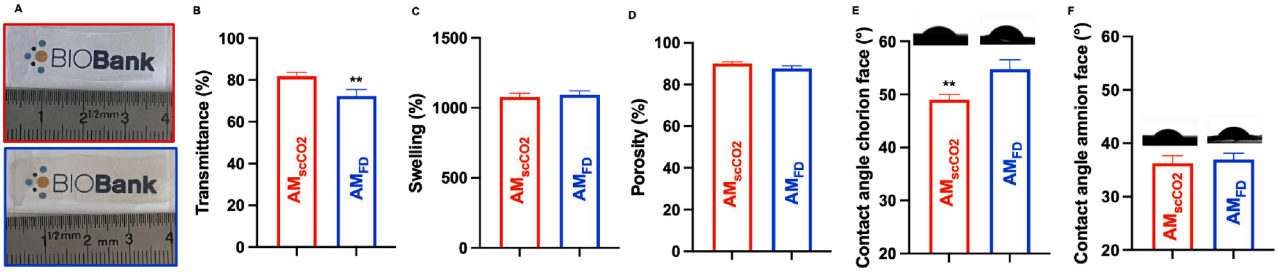

Fig. 2. Structural and physicochemical characterization of m-Supercrit® processed amniotic membrane (AM_{scCO2}; highlighted in red) and freeze-dried amniotic membrane (AM_{FD}; highlighted in blue). A: Macroscopical views of hydrated AM samples. Histograms showing the transmittance of the samples at 650 nm (B), the water retention (C), total porosity (D) and wettability (E and F) of the samples. Inserts show the droplet shape. ((**) $p < 0.01$, Mann-Whitney test, n = 4). (For interpretation of the references to colour in this figure legend, the reader is referred to the web version of this article.)

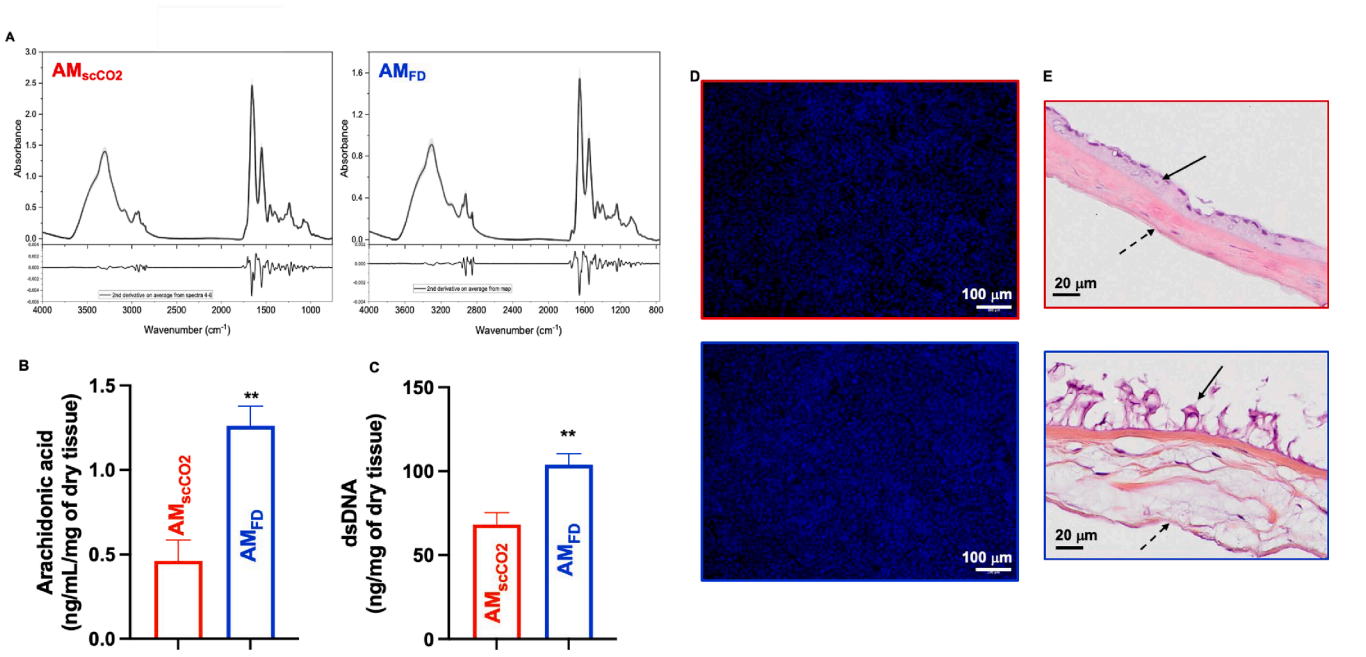

Fig. 3. Characterization of m-Supercrit® processed amniotic membrane (AM_{scCO2}; highlighted in red) and freeze-dried amniotic membrane (AM_{FD}; highlighted in blue) performed by infrared micro spectroscopy (A). Inserts indicate the second derivatives of the IR spectra. Histograms showing AA content (B) and residual double-stranded DNA (C) of the samples ((**) $p < 0.01$, Mann-Whitney test, $n = 4$). Fluorescent microscopy visualisation of DAPI stained nuclei (D, scale bars = 100 µm) and HES staining of paraffin embedded sections (E, scale bars = 20 µm). black arrows indicate the amniotic side and dashed arrows indicate the chorion side. (For interpretation of the references to colour in this figure legend, the reader is referred to the web version of this article.)

basement membrane components in comparison to AM_{FD} (Fig. 3E). Taken together, these results indicate that the m-Supercrit® process doesn't achieve complete decellularization of the AM. Additional steps using detergent should be introduced to achieve a complete decellularisation of the AM. Despite the efficient lipid extraction capability of $scCO_2$, m-Supercrit® processing likely requires combination with detergents to ensure full nuclear removal from AM, as reported previously. [26,27] Preserved AM is commonly considered to be an inert tissue, with no viable cells.[28] The vitality of residual cells within the m-Supercrit® processed AM was also assessed. Neither cell metabolic activity nor cell migration from AM explants are observed (Figure SI-2), indicating that the m-Supercrit® process produces devitalized, inert AM.

Consistent with the TGA results, showing that AM exhibits thermal characteristics similar to collagen,[20] the overall shape of the IR spectra of AM (Fig. 3A) closely resembles those reported for collagen. [27] Both AM_{scCO2} and AM_{FD} spectra display major bands around 1656 and 1551 cm^{-1}, corresponding primarily to the amide I and II bands of collagen, respectively. The amide I band is particularly sensitive to collagen secondary structure. Second derivative spectra reveal two principal bands at 1694 and 1659 cm^{-1} for AM_{scCO2} and at 1691 and 1655 cm^{-1} for AM_{FD} (Fig. 3 A, insert), assigned to β-turns and β-sheets of collagen, respectively.[29] In addition to these spectral shifts, changes in the relative intensities of the amide I bands at ~ 1657 and 1633 cm^{-1} suggest alterations in collagen secondary structure following m-Supercrit® processing. Qualitative Masson's Trichrome staining confirms that AM_{scCO2} predominantly contains collagen, similarly to AM_{FD} (Fig. 4A). To further evaluate collagen integrity, second harmonic generation (SHG) imaging was performed. The presence of the SHG pattern in AM_{scCO2} indicates the persistence of fibrillar collagen.[12] AM_{scCO2} exhibits a randomly organized SHG pattern comparable to that of AM_{FD}. However, a significant reduction in SHG signal is observed in AM_{scCO2} compared to that of AM_{FD} (0.14 ± 0.06 *vs.* 0.29 ± 0.09grey level/μm^2, respectively, $p < 0.01$, Mann-Whitney, Fig. 4B-C). A decrease in SHG signal intensity has been correlated with significant disruption in decellularized tissue.[30] Therefore, a deeper characterization of the collagen matrix was performed on pepsin-digested AM (Fig. 4D). Protein and collagen quantifications show a significant decrease in the collagen content in AM_{scCO2} compared to that of AM_{FD} (261 ± 11 *vs.* 423 ± 51 mg/g of dry mass, respectively, $p < 0.02$, Mann-Whitney, Fig. 4E), in line with total protein quantification (Fig. 4F). Circular dichroism spectroscopy performed on pepsin-digested AM samples shows that collagen from AM_{scCO2} doesn't exhibit the characteristic spectral features of collagen triple helix *i.e.,* a positive band at 222 nm (n –> π* transition of amide backbone) followed by a negative band at 195–200 nm (associated to π-π* transition of amide backbone).[31] Unlike AM_{FD}, AM_{scCO2}-derived collagen displays alterations in the sinusoidal pattern by the disappearance of the negative peak at 195–200 nm (Fig. 4G). The persistence of positive peaks, characteristic of random polypeptide chain conformations, suggests partial collagen unfolding following m-Supercrit® processing.[32] Taken together, these results confirm an alteration in the collagen matrix of AM_{scCO2}. A multi-step optimization strategy based on Quality-by-Design should be implemented to further improve the process while minimizing collagen matrix degradation.

IR spectra also exhibit absorption bands in the 1170 and 800 cm^{-1} regions, arising mainly from the νC-O, νC-C, νC-O-C vibration associated with carbohydrate moieties, as well as νsPO_2 (nucleic acids, phospholipids) and νsSO_2 (GAGs).[33] GAGs are negatively charged biopolymers that can be classified into sulfated GAGs, such as chondroitin sulfate/dermatan sulfate, heparan sulfate, and keratan sulfate, and non-sulfated GAG such as hyaluronic acid (HA). Compared with AM_{FD}, the spectra of AM_{scCO2} shows marked alteration of the fingerprint region, indicating a partial loss or modification of GAGs content. Qualitative Alcian Blue staining demonstrates that AM_{scCO2} contains non-sulfated and sulfated GAGs, similarly to AM_{FD} (Fig. 4H). Quantitative analyses of GAGs were performed on proteinase K and papain-digested samples (Fig. 4D). While no significant difference in HA content is observed in proteinase K digests (38 ± 12 *vs.* 71 ± 17 mg/g of dry mass, Fig. 4I), an expect increase in sulfated GAGs is detected in papain AM_{scCO2} digest (13.45 ± 0.68 *vs.* 8.85 ± 0.76 mg/g of dry mass, $p < 0.02$, Mann-Whitney, Fig. 4J), a phenomenon consistent with depolymerisation of sulfated GAGs.[34] AM provides mechanical support during fetal development and exhibits high mechanical strength and elasticity.[35] The linear elastic

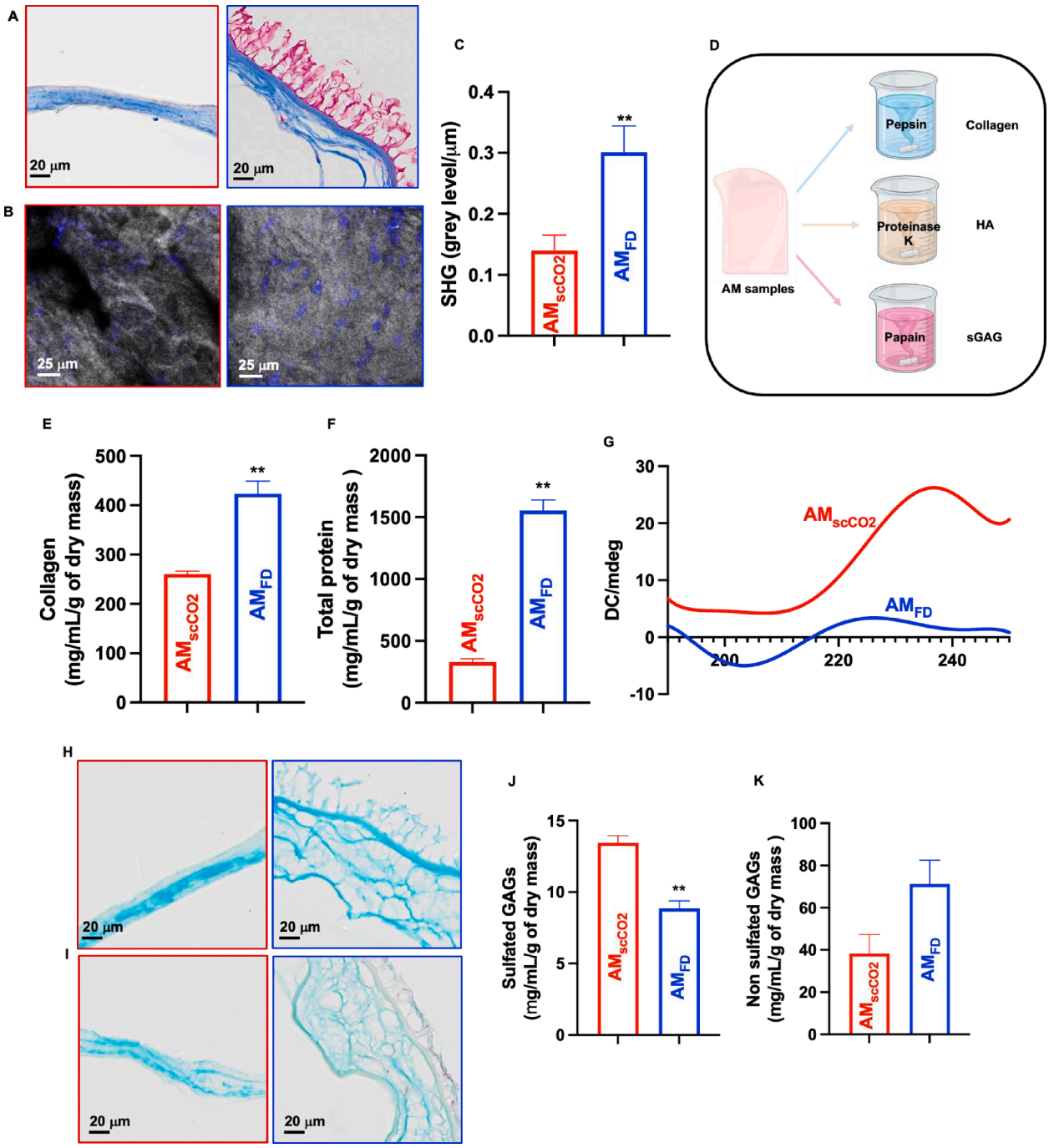

Fig. 4. Biochemical composition of m-Supercrit® processed amniotic membrane (AM_{scCO2}; highlighted in red) and freeze-dried amniotic membrane (AM_{FD}; highlighted in blue). Masson's staining of paraffin embedded sections (A, scale bars = 20 µm) and SHG (B; scale bars = 50 µm). Blue dots indicate DAPI stained nuclei. Histograms showing SHG signal quantification (C). Methodological procedure for AM digestion (D). Histograms indicating the collagen (E), protein content (F) and circular dichroism (G) in pepsin-digested samples. Alcian blue staining of paraffin embedded sections at pH1.5 and 2.5 (respectively H and I, scale bars = 20 µm). Histograms indicating sGAGs content in papain digested samples (J) and HA content in proteinase K digested samples (K). (**) $p < 0.02$, n = 4, Mann Whitney test. (For interpretation of the references to colour in this figure legend, the reader is referred to the web version of this article.)

modulus—defined as the slope of the initial linear region of the stress–strain curve— was measured under dry and wet conditions, using an average strain load of 2% to avoid sample damage (Fig. 5A). As for AM_{FD}, AM_{scCO2} samples exhibit non-linear behavior during uniaxial testing. Despite the reduced thickness of AM_{scCO2} (Fig. 1D), a significant increase in the linear elastic modulus is observed in both dry and wet states. (Fig. 5B-C) AM_{scCO2} exhibits values of 126 ± 27 MPa (dry) and 4.75 ± 1.57 MPa (wet), higher than those obtained for AM_{FD}; 77 ± 4.55 MPa (dry, $p < 0.0007$, Mann-Whitney) and 0.71 ± 0.24 MPa (wet, $p <$ 0.002, Mann-Whitney). The increased stiffness of AM_{scCO2} may be attributed to alterations in collagen organization, as reported above.

Biodegradability of AM is a critical parameter for tissue healing. Collagenase and hyaluronidase are commonly used to partially mimic *in vivo* biodegradation of collagen- and hyaluronic acid-based tissues.[36] In this study, the impact of the m-Supercrit® process on AM degradation was evaluated by incubating samples with collagenase and hyaluronidase. Similar to AM_{FD}, AM_{scCO2} is completely degraded after 72 h in collagenase, with only negligible residual material recovered. When

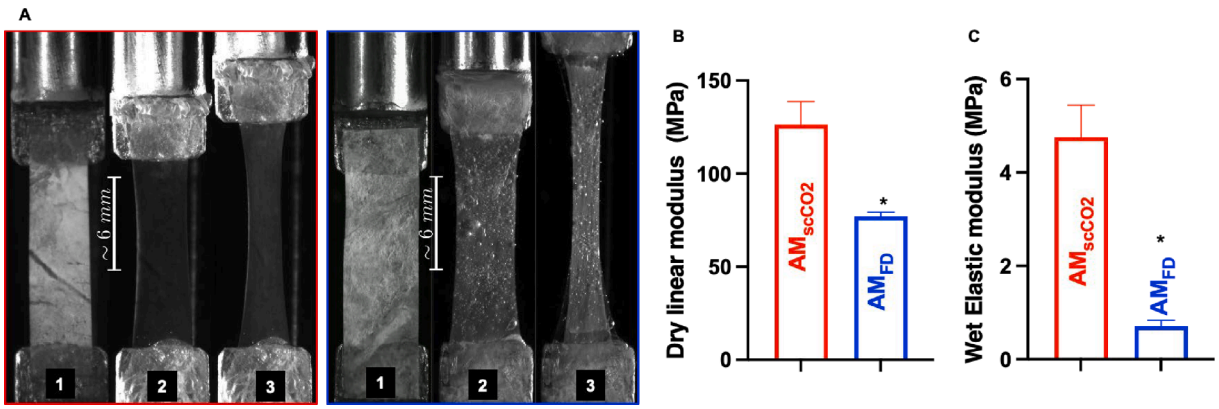

Fig. 5. Mechanical response of m-Supercrit® processed amniotic membrane (AM_{scCO2}; highlighted in red) and freeze-dried amniotic membrane (AM_{FD}; highlighted in blue). Macroscopical views of AM samples in dry (A1) and wet (A2 and 3) conditions. A2 at the initial state and A3 at the final state, scale bars = 6 μm. Histograms showing the linear elastic modulus of AM samples in dry (B) and wet (B) conditions. (*) $p < 0.002$, n = 6, Mann Whitney test. (For interpretation of the references to colour in this figure legend, the reader is referred to the web version of this article.)

incubated in hyaluronidase, AM_{scCO2} exhibits a weight loss of 21 ± 9%, comparable to that of AM_{FD} 34 ± 5% (Fig. SI-3). Despite the biochemical modifications induced by m-Supercrit® processing, the enzymatic degradation of AM is therefore not significantly altered.

3.3. Biocompatibility of m-Supercrit® processed-AM

AM allografts have been used across multiple medical fields since the early 20th century. Several studies have demonstrated that the presence of viable cells within the AM is not strictly required for therapeutic efficacy.[37] Instead, ECM-derived AM is believed to support stromal cell recruitment and tissue repair. From a regulatory standpoint, allografts are classified by health authorities as human cell or tissue products and therefore do not require approval under an investigational new drug application or device exemption.[17] Nevertheless, biocompatibility testing is mandatory prior to the clinical use.[38] Moreover, although PAA has a low toxicity, a residual PAA of 0.22 ± 0.04 mg/mL, below a detection limit, was detected in AMscCO2 process. Due to their high volatility and rapid decomposition during depressurization residual H_2O_2 and ethanol were not investigated. Therefore, accordingly, the hemocompatibility and cytocompatibility of AM_{scCO2} were evaluated in compliance with ISO/EN 10,993 part 4 and 5 guidelines. The hemolytic rate of both AM_{scCO2} and AM_{FD} is below 5%, which is the threshold defined by ASTM F 756–2000, indicating favourable blood compatibility. (Fig. 6A) Dermal fibroblast viability in the presence of AM_{scCO2} and AM_{FD} extracts remains above the 70% threshold, (Fig. 6B). We showed above (Fig. 3E) that AM_{scCO2} has better preserved basement membrane components, and is therefore considered more suitable for cell cultivation.[39] The ability of fibroblasts to adhere and proliferate on AM_{scCO2} was also assessed (Fig. 6C and SI-4). As shown in the Fig. SI-4, fibroblasts adhere and spread on the surface of AM_{scCO2}. Semi-quantitative morphological analysis reveals a significant increase in fibroblast spreading area on AM_{scCO2} (1,213 ± 411 μm^2) compared with AM_{FD} (835 ± 295 μm^2, $p < 0.003$, Mann-Whitney, Fig. SI-4). WST-1® proliferation assays demonstrate sustained fibroblast proliferation over prolonged culture period (Fig. 6C). After 10 days of culture, SEM and confocal laser microscopy reveal that fibroblasts exhibit elongated morphology and anisotropic organisation on AM_{scCO2} (Fig. 6D-E, upper pictures). Interestingly, on AM_{FD} fibroblasts are also elongated but with isotropic organisation (Fig. 6D-E, lower pictures), probably due to the presence of disturbed epithelial cell monolayer beneath the seeded fibroblast. Taken together, these results indicate a good cytocompatibility of AM_{scCO2}.

Sulfated GAGs play a key role in regulating the localization and activity of growth factors through their polysaccharide backbone and the spatial arrangement of sulfate groups. However, over-sulfation of GAGs (as described above) has been reported to reduce growth factor availability and bioactivity.[40] On the other hand, the partial decellularization induced by m-Supercrit® process may contribute to the removal of cell-associated components, including growth factors. This prompted

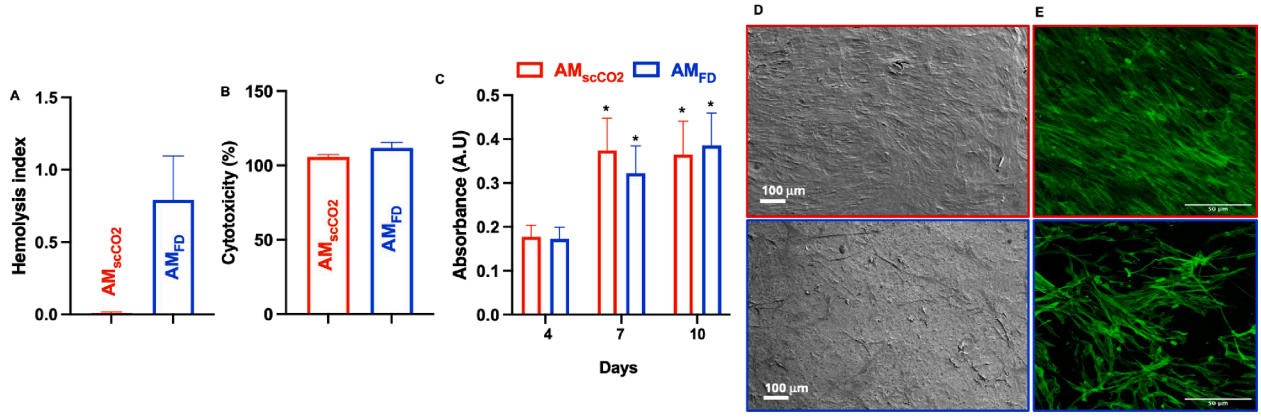

Fig. 6. Hemocompatibility and cytocompatibility of m-Supercrit® processed amniotic membrane (AM_{scCO2}; highlighted in red) and freeze-dried amniotic membrane (AM_{FD}; highlighted in blue). Histograms showing hemocompatibility (A), cytocompatibility (B) and fibroblast proliferation (C) of/on AM samples. (*) *vs.* day 4, $p < 0.02$, n = 6, Mann Whitney test. SEM (D) and confocal microscopy observation of cytoskeleton-labelled fibroblasts (E). Scale bars = 100 and 50 μm, respectively. (For interpretation of the references to colour in this figure legend, the reader is referred to the web version of this article.)

an investigation into the bioavailability of growth factors in AM_{scCO2}. Indeed, upon exposure to biological fluids, ECM-resident growth factors are released, thereby contributing to AM bioactivity. In vivo, ECM-resident growth factor availability is likely to occur progressively through enzymatic degradation of the ECM and interactions with surrounding tissues. To estimate the remaining bioactive factor content within AM_{scCO2}, AM_{scCO2} and AM_{FD} were grinded and soaked in DMEM culture media for 48 h and the released ECM-resident growth factors were quantified by ELISA as previously described.[12] Vascular endothelial growth factor (VEGF), basic fibroblast growth factor (b-FGF) hepatic growth factor (HGF), insulin growth factor (IGF), and basic transforming growth factors beta (TGF-β) are detected in the conditioned media (Table 2). While no significant differences are observed in the passive release of VEGF, TGF-β and IGF between the two samples, a significant reduction in the release of b-FGF and HGF is measured for AM_{scCO2}, suggesting that the m-Supercrit® process partially reduces AM bioactivity and pro-healing capabilities. Notably, in corneal reconstruction –one of its most prominent fields of application of AM– the anti-angiogenic properties of AM are highly desirable.[41] The low release of VEGF and the absence of b-FGF observed in AM_{scCO2} may be beneficial for limiting neovascularization and preserving corneal transparency. Beyond growth factor release profiling, we examined the effects of AM extracts on fibroblast migration and wound healing, given the key roles of b-FGF and HGF in simulating cell motility.[42] Compared with AM_{FD}, the AM_{scCO2} extract induces a significantly lower wound-healing response. ($p < 0.0001$, Mann-Whitney, Fig. 7A-B) At 72 h post-scratching, wound closure reaches only 44 ± 7% in the presence of AM_{scCO2} extracts, compared with 97 ± 4% for AM_{FD} ($p < 0.0001$, Mann-Whitney, Fig. 7C). These results confirm that m-Supercrit® process reduces AM bioactivity. Nevertheless, the preservation of the ECM architecture and other bioactive components may still support cellular interactions and tissue repair. Further studies will be necessary to evaluate the functional impact of this reduction in relevant biological models.

AM extracts have previously been reported to exert anti-proliferative effects on cancer cells.[43] This property was investigated here using MDA-MB231 breast cancer cells. WST-1® assay performed after 24 h of exposure reveals a marked decrease in MDA-MB231 cell viability in the presence of AM_{scCO2}, falling below 50%, whereas MDA-MB231 cell viability remains above 90% in the presence of AM_{FD} compared with MDA-MB231 cell control ($p < 0.001$, *t*-test, Fig. 7D). After 72 h, both AM samples significantly reduce cancer cell viability, reaching 16% for AM_{scCO2} and 38% for AM_{FD} ($p < 0.001$, *t*-test, Fig. 7D). These results indicate that AM reduces breast cancer cell viability and that this anti-proliferative effect is enhanced by m-Supercrit® processing. Importantly, AM_{scCO2} does not adversely affect dermal fibroblast growth (Fig. 6C). Further studies are required to elucidate the molecular mechanisms underlying the anti-proliferative activity of AM.

The innate immune system plays a central role in host defence against foreign materials. Although perinatal tissues are generally characterized by low immunogenicity,[44] m-Supercrit® processing may generate ECM-derived peptides that could be recognized by inflammatory cells as damage-associated molecular patterns. Polynuclear Neutrophils (PNN), which act as first responders during host defence, can produce large amounts of reactive oxygen species (ROS), potentially triggering excessive inflammation. PNN respiratory burst activity, assessed as intracellular ROS accumulation, was therefore evaluated in response to AM_{scCO2}. Data were normalized to basal ROS production to account for inter-donor variability. Flow cytometry analysis shows no PNN activation upon contact with either AM_{scCO2} or AM_{FD}, as no increase in intracellular ROS is detected (Fig. 8A). We previously reported that Wharton's jelly, another perinatal tissue derivative, can attenuate lipopolysaccharide (LPS)-induced PNN activation.[12] Accordingly, the potential synergistic effects of AM and LPS were investigated. No cumulative effect of LPS and AM samples on ROS accumulation is observed. (Fig. 8B). IL-8 levels in PNN supernatants were also quantified. Neither AM_{scCO2} nor AM_{FD} alone induces IL-8 release (Fig. 8C). While no synergistic effect of LPS and AM_{scCO2} on IL-8 secretion is observed, a significant increase in IL-8 release—at least threefold ($p < 0.02$, Mann-Whitney, Fig. 7B)—is detected following co-stimulation with AM_{FD} and LPS.

Monocytes are subsequently recruited to the implantation site and differentiate into macrophages, which play a pivotal role in modulating inflammation and tissue repair. The balance between pro- and anti-inflammatory cytokines is critical for appropriate healing responses. Pro-inflammatory cytokines such as tumor necrosis factor-α (TNF-α) are typically released during early inflammatory phases, whereas anti-inflammatory mediators such as interleukin-10 (IL-10) suppress the biomaterial-induced inflammatory response and contribute to resolution and tissue repair.[45] In this study, the effects of AM_{scCO2} on TNF-α and IL-10 secretion by U937-derived macrophages were evaluated after 4 and 24 h of contact. Macrophages stimulated with LPS served as positive controls. TNF-α levels in the presence of both AM_{scCO2} and AM_{FD} remain below 1 ng/mL, at least 2.7-fold lower than those induced by LPS (Fig. 9A). In contrast, IL-10 release exceeds 50 pg/mL after 4 h and increases significantly after 24 h (at least 6-fold; $p < 0.007$, Mann-Whitney, Fig. 9B). The TNF-α/IL-10 ratio, used as an indicator of the pro-to-anti-inflammatory balance, remains below 1 and decreases over time, indicating that AM_{scCO2} does not provoke excessive inflammatory responses (Fig. 9C). Interestingly, these levels are lower than those of unstimulated U937. Given the well-documented anti-inflammatory properties of perinatal tissue derivatives,[46] macrophages were also exposed to combined AM and LPS stimulation. Although both TNF-α and IL-10 levels were significantly increased under co-stimulation conditions (Fig. 9D-E), the TNF-α/IL-10 ratio, initially above 1 at 4 h, decreases below 1 at 24 h. TNF-α/IL-10 ratio for AM_{FD} is at least two times higher than AM_{scCO2} ($p < 0.0001$, Mann–Whitney, Fig. 9F), but remains lower than LPS control. These findings demonstrate that m-Supercrit® processing preserves the intrinsic anti-inflammatory properties of the amniotic membrane.

Table 2
Released growth factors from amniotic membrane samples.

pg/mL	AM_{scCO2}	AM_{FD}	Mann & Whitney
VEGF	6.75 ± 3.06	2.80 ± 0.85	$p = 0.34$
HGF	114.9 ± 61	9753.4 ± 2573.6	$p = 0.001$
b-FGF	ND	742.6 ± 386.7	$p = 0.0003$
IGF	1429.11 ± 559.65	893.4 ± 59.8	$p = 0.11$
TGF-β	306.78 ± 87.55	425.03 ± 187.75	$p = 0.39$

Abbreviations: VEGF: vascular growth factor, HGF: hepatocyte growth factor, b-FGF: basic fibroblast growth factor, IGF: insulin-like growth factor, TGF-β: Transforming growth factor beta.

3.4. Towards clinical application: proof of concept

The aforementioned results indicate that AM_{scCO2} exhibits physico-chemical and biological properties particularly suited for ophthalmologic applications, including enhanced transparency, increased elastic modulus, and reduced levels of HGF and b-FGF. In European countries, such as France, the clinical use of AM is currently restricted to ophthalmology, as the eye is considered an immune-privileged site.[44] Based on these observations, we sought to evaluate the feasibility of using AM_{scCO2} in a clinically relevant surgical context by assessing its ability to be sutured onto the corneal surface (Fig. 10A). Porcine ocular globes were regularly obtained from a local slaughterhouse. In accordance with current regulations (EU Directive 2010/63/EU), no ethical committee approval was required, as no animals were specifically sacrificed for research purposes.[47] AM samples were sutured onto the cornea using standard ophthalmic 10–0 surgical sutures. Compared with AM_{FD}, AM_{scCO2} exhibits markedly improved handling properties during suturing, likely attributable to its increased stiffness (Fig. 10B, arrows). Histological analysis of Masson's trichrome–stained paraffin sections

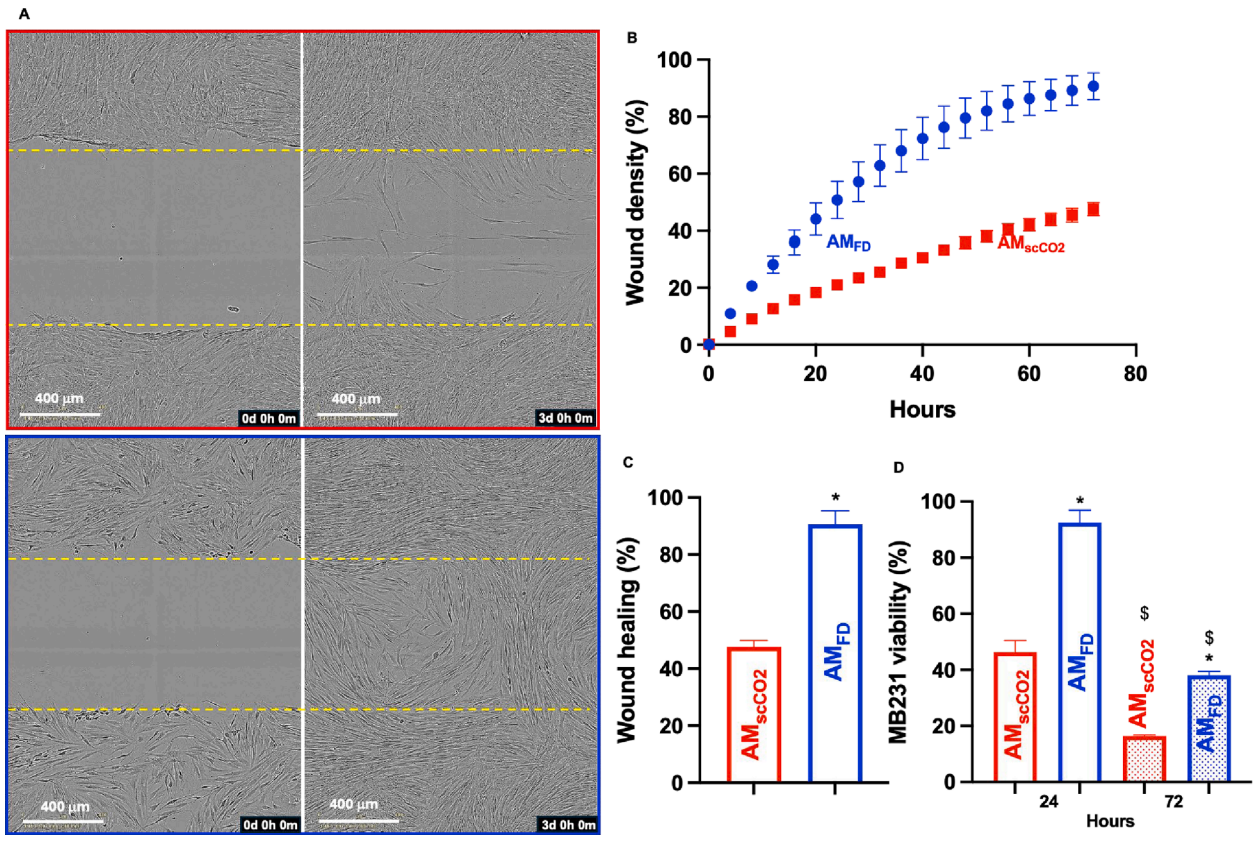

Fig. 7. Bioactivity of m-Supercrit® processed amniotic membrane (AM_{scCO2}; highlighted in red) and freeze-dried amniotic membrane (AM_{FD}; highlighted in blue). Incucyte® pictures showing the wound at the beginning (left) and the end (right) of the wound healing assay test (scale bars = 400 µm). Curves showing the kinetic of wound recovery (B). Histograms showing MDA-MB231 viability at 24 and 72 h of culture in the presence of AM samples. (*) *vs* AM_{scCO2} $p < 0.0001$, ($) *vs* 24 h, $p < 0.0001$, n = 3, *t*-test. (For interpretation of the references to colour in this figure legend, the reader is referred to the web version of this article.)

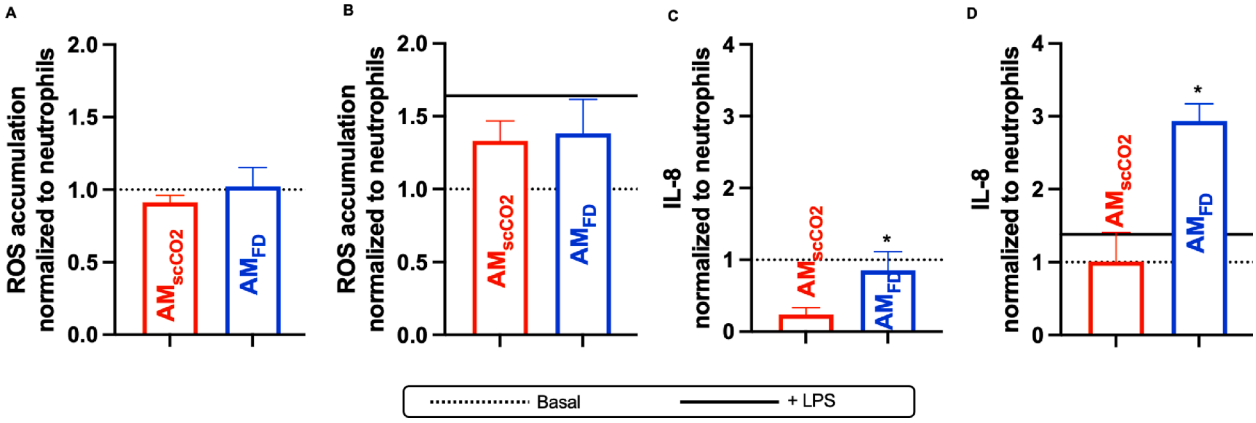

Fig. 8. Innate neutrophile response to m-Supercrit® processed amniotic membrane (AM_{scCO2}; highlighted in red) and freeze-dried amniotic membrane (AM_{FD}; highlighted in blue). Histograms showing intracellular accumulation of reactive oxygen species in basal (A) and LPS co-stimulated cells (B). Histograms showing IL-8 release in basal (C) and LPS stimulated cells (D). Dashed lines indicate the basal production by PNN and back lines indicate LPS-responses. (*) $p < 0.02$, n = 5, Mann-Whitney. (For interpretation of the references to colour in this figure legend, the reader is referred to the web version of this article.)

confirmed the presence and stable positioning of AM_{scCO2} in close apposition to the corneal tissue. Taken together, these results demonstrate the feasibility of handling and suturing AM_{scCO2} in a clinically relevant ophthalmic setting, supporting its further evaluation in preclinical models for corneal repair applications. Future studies, particularly *in vivo* models such as corneal epithelial defect healing, will be necessary to determine whether these preserved properties can compensate for the decreased growth factor content. Furthermore, post-processing functionalization strategies could be explored to restore or enhance bioactivity, including the incorporation of exogenous growth factors or bioactive molecules onto the ECM scaffold without compromising sterility.

4. Conclusion

In this study, we present a sterile, devitalized amniotic membrane produced using the m-Supercrit® process, which markedly shortens the manufacturing timeline compared with conventional preservation

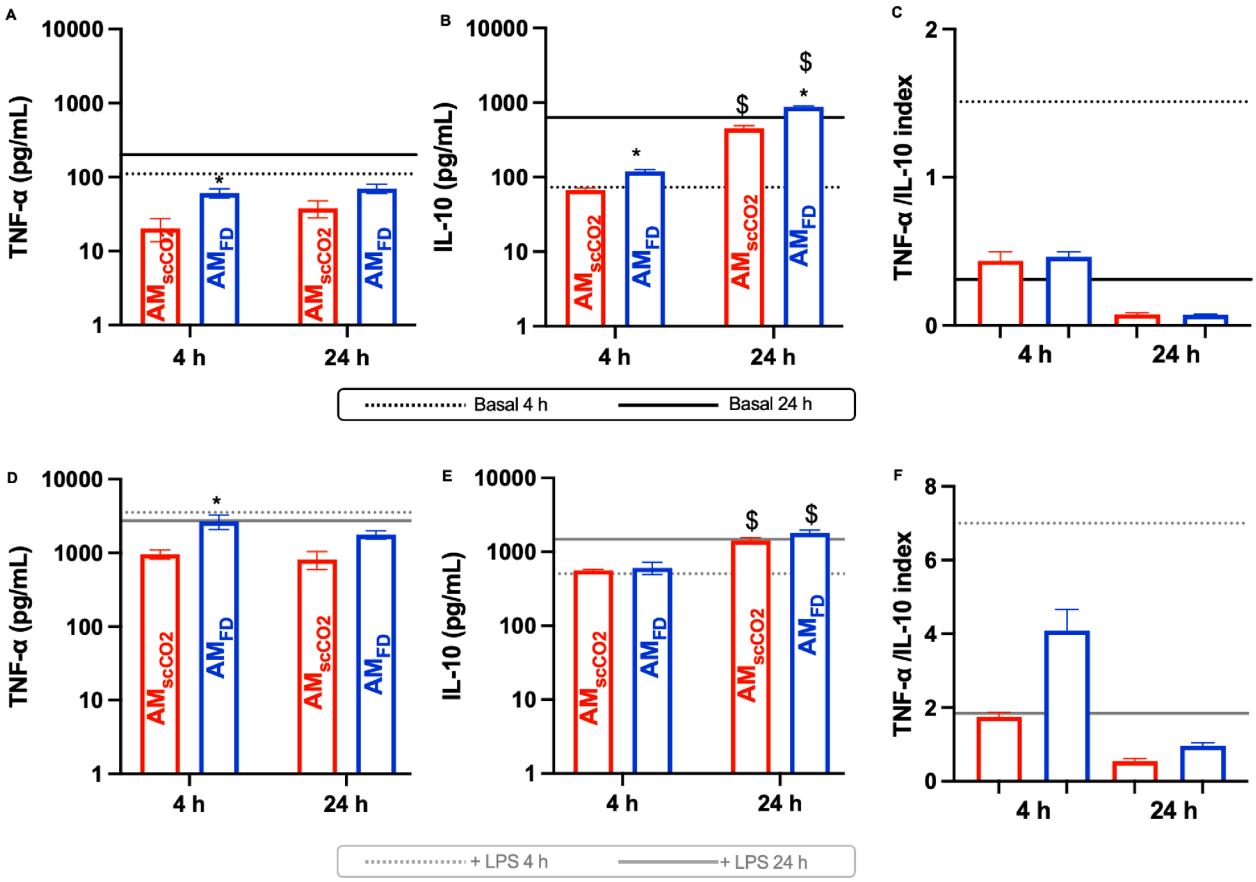

Fig. 9. Macrophage response to m-Supercrit® processed amniotic membrane (AM_{scCO2}; highlighted in red) and freeze-dried amniotic membrane (AM_{FD}; highlighted in blue). Histograms showing TNF-a (A, D), IL-10 (B, E) release from U937 differentiated macrophages and the TNF-a/IL-10 index (C, F). Upper row in the absence of LPS co-stimulation. Dashed and solid lines indicate the basal production of cytokines in the absence of AM samples at 4 and 24 h, respectively. Lower row in the presence of LPS-co-stimulation. Dashed and solid lines indicate the basal production of cytokines in the absence of AM samples at 4 and 24 h, respectively. (*) *vs.* AM_{scCO2} $p < 0.007$, ($) *vs.* 4 h $p < 0.0001n = 6$, Mann-Whitney. (For interpretation of the references to colour in this figure legend, the reader is referred to the web version of this article.)

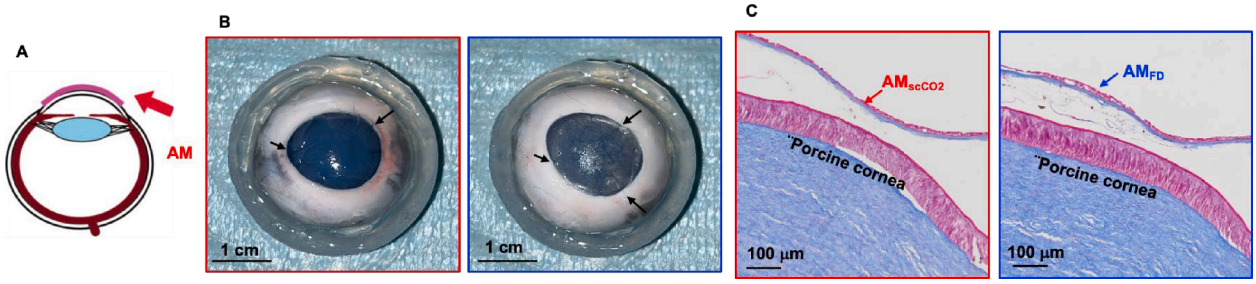

Fig. 10. Ex vivo suture test onto the corneal surface of m-Supercrit® processed amniotic membrane (AM_{scCO2}; highlighted in red) and freeze-dried amniotic membrane (AM_{FD}; highlighted in blue). Methodological procedure for ophthalmic application (A). Pictures showing AM samples sutured to porcine ocular globes. Black arrows indicate the sutures (B, scale bars = 1 cm). Masson's staining of paraffin-embedded sections (C, scale bars = 100 µm). (For interpretation of the references to colour in this figure legend, the reader is referred to the web version of this article.)

methods. m-Supercrit® processing induces structural changes in the tissue, characterized by reduced thickness, which, in turn, drives significant alterations in biochemical composition and mechanical behavior, including increased stiffness while maintaining high transparency and low residual moisture. Functionally, these structure–property changes preserve overall biocompatibility while modulating biological activity, resulting in reduced pro-angiogenic growth factors, enhanced antiproliferative effects on cancer cells, and pronounced anti-inflammatory responses in neutrophils and macrophages. From a clinical perspective, these combined physicochemical and biological features support the use of m-Supercrit®-processed amniotic membrane as a mechanically robust, transparent, and immunomodulatory barrier. A reduction in certain growth factors, including HGF and b-FGF could potentially affect the pro-healing performance of the membrane. Nevertheless, the preservation of the ECM architecture and other bioactive components still support cellular interactions and tissue repair. Further studies will be necessary to evaluate the functional impact of this reduction in relevant biological models. With further optimization of process parameters to limit matrix degradation, the m-Supercrit® process represents a viable pathway toward the development

of an off-the-shelf sterile amniotic membrane for corneal repair applications.

CRediT authorship contribution statement

L. Adam: Writing – review & editing, Data curation, Conceptualization. **S. Rota:** Writing – review & editing, Methodology, Funding acquisition, Data curation, Conceptualization. **F. Lemaire:** Writing – review & editing, Data curation, Conceptualization. **C. Guillaume:** Supervision, Data curation, Conceptualization. **N. Bouland:** Supervision, Data curation, Conceptualization. **A. Da Rocha:** Writing – review & editing, Data curation, Conceptualization. **A. Baldit:** Writing – review & editing, Validation, Data curation, Conceptualization. **Q. Bourgogne:** Writing – review & editing, Validation, Supervision, Data curation, Conceptualization. **J. Rodon-Fores:** Writing – review & editing, Validation, Supervision, Data curation, Conceptualization. **F. Quilès:** Writing – review & editing, Formal analysis, Data curation, Conceptualization. **C. Mauprivez:** Writing – review & editing, Validation, Supervision, Formal analysis, Data curation, Conceptualization. **R. Bardonnet:** Writing – review & editing, Project administration, Methodology, Investigation, Funding acquisition, Conceptualization. **H. Kerdjoudj:** Writing – original draft, Validation, Supervision, Methodology, Funding acquisition, Formal analysis, Data curation.

Declaration of competing interest

The authors declare that they have no known competing financial interests or personal relationships that could have appeared to influence the work reported in this paper.

Acknowledgements

Association Nationale Recherche Technologique (ANRT) is acknowledged for financial support. Authors are grateful to the staff of Reims Maternity Hospital for providing placenta and to the staff of pediatric surgery department of Reims hospital for providing foreskin explants and to the staff of the Core PICT (Dr. C. Terryn), URCACyt (Dr. S. Audonnet), Spectroscopy and Microscopy Service Facility (SMI) of LCPME, MécaRhéo as well as MicroMat of LEM3, and corresponding equipment availability. Authors also thank Dr. E. Krawiec for corneal sutures and Dr. L. Van Gulick and Pr. H. Morjani for providing MDA-MB231 breast cancer cells their help and suggestions.

Appendix A. Supplementary data

Supplementary data to this article can be found online at https://doi.org/10.1016/j.matdes.2026.115964.

Data availability

Data will be made available on request.

References

[1] J.S. Davis, Skin Grafting at the Johns Hopkins Hospital, Ann. Surg. 50 (1909) 542–554.
[2] A. de Rothh, Plastic repair of conjunctival defects with fetal membranes, Arch. Ophthalmol. 23 (1940) 522–525.
[3] A. Hopkinson, F.C. Figueiredo, A Narrative Review of Amniotic Membrane Transplantation in Ocular Surface Repair: Unveiling the Immunoregulatory Pathways for Timely intervention, Ophthalmol. Ther. 14 (2025) 1385–1409.
[4] N. Hofmann, X. Lafarge, M. Antica, N. Ferry, L. Girandon, R. Gramignoli, M. Jurga, H. Kerdjoudj, R. Navakauskiene, J. Schiavi, V. Shablii, F.J. Nicolàs, F. Gindraux, Expert Consideration on Regulatory Aspects for Perinatal Derivatives in Clinical Settings, Stem Cells Transl. Med. 12 (2023) 258–265.
[5] B. Fantaci, B. Calvo, A.M. Mesa, A. Ortillés, Comparative evaluation of the mechanical properties of amniotic membranes for corneal grafting: Effects of cryopreservation, lyophilization, and dehydration, J. Mech. Behav. Biomed. Mater. 173 (2026) 107234.
[6] R. Gramignoli, N. Hofmann, M. Agudo-Barriuso, M. Antica, A.I. Flores, L. Girandon, H. Kerdjoudj, R. Navakauskiene, J. Schiavi, H. Scholz, V. Shablii, X. Lafarge, F.J. Nicolàs, F. Gindraux, Expert Revision of Key elements for Clinical-Grade Production and Qualification of Perinatal Derivatives, Stem Cells Transl. Med. 13 (2024) 14–29.
[7] N. Ahmed, V. Eras, A. Pruß, C. Perka, J. Brune, T.L. Vu-Han, Allografts: expanding the surgeon's armamentarium, Cell Tissue Bank. 24 (2023) 273–283.
[8] A. Tabernero, A. González-Garcinuño, S. Cardea, E. Martín del Valle, Supercritical carbon dioxide and biomedicine: opening the doors towards biocompatibility, Chem. Eng. J. 444 (2022) 136615.
[9] R.J.J. de Wit, D.J. van Dis, M.E. Bertrand, D. Tiemessen, S. Siddiqi, E. Oosterwijk, A.F.T.M. Verhagen, Scaffold-based tissue engineering: Supercritical carbon dioxide as an alternative method for decellularization and sterilization of dense materials, Acta Biomater. 155 (2023) 323–332.
[10] J.S. McDaniel, J.L. Wehmeyer, L.E. Cornell, A.J. Johnson, D.O. Zamora, Amniotic membrane allografts maintain key biological properties post SCCO2 and lyophilization processing, J. Biomater. Appl. 35 (2021) 592–601.
[11] M. Fénelon, S. Catros, C. Meyer, J.C. Fricain, L. Obert, F. Auber, A. Louvrier, F. Gindraux, Applications of Human Amniotic Membrane for Tissue Engineering, Membranes 11 (2021) 387.
[12] M. Dubus, L. Scomazzon, J. Chevrier, A. Montanede, A. Baldit, C. Terryn, F. Quilès, C. Thomachot-Schneider, S.C. Gangloff, N. Bouland, F. Gindraux, H. Rammal, C. Mauprivez, H. Kerdjoudj, Decellularization of Wharton's Jelly increases its Bioactivity and Antibacterial Properties, Front. Bioeng. Biotechnol. 10 (2022) 828424.
[13] A. Lavrand, L. Adam, A. Da Rocha, F. Lemaire, C. Loth, A. Baldit, M. Vasseaux, L. Van Gulick, A. Beljebbar, P. Augusto, A. Berquand, C. Salameh, N. Nassif, F. Boulmedais, C. Mauprivez, E. Brenet, H. Kerdjoudj, Hydrogels from Wharton's jelly as alternative to conventional extracellular matrix-based constructs, Int. J. Biol. Macromol. 328 (2025) 147552.
[14] F.J. Verdugo-Avello, J.K. Wychowaniec, M. Jimenez, S. Jimenez, S. Gutierrez, Current concepts for tissue transplant services for developing countries, Cell Tissue Bank. 22 (2021) 323–337.
[15] R.J. Lomas, J.E. Cruse-Sawyer, C. Simpson, E. Ingham, R. Bojar, J.N. Kearney, Assessment of the biological properties of human split skin allografts disinfected with peracetic acid and preserved in glycerol, Burns 29 (2003) 515–525.
[16] Q.Q. Qiu, P. Leamy, J. Brittingham, J. Pomerleau, N. Kabaria, J. Connor, Inactivation of bacterial spores and viruses in biological material using supercritical carbon dioxide with sterilant, J. Biomed. Mater. Res. B Appl. Biomater. 91 (2009) 572–578.
[17] M.C. Moore, A. Van De Walle, J. Chang, C. Juran, P.S. McFetridge, Human Perinatal-Derived Biomaterials, Adv. Healthc. Mater. 6 (2017) 1700345.
[18] N. Asaithambi, A. Tuhanioglu, A. Ubeyitogullari, A novel drying technology based on supercritical carbon dioxide to enhance the functional properties of red lentil proteins, Future Foods 12 (2025) 100842.
[19] H. Suroto, I. Pratamanugroho, T. Prajasari, H. Susilowati, G. Khang, Analysis of morphology, cytotoxicity, and water content characteristics of freeze-dried amnion membrane from human and bovine, Narra J 4 (2024) e991.
[20] R. Durga, N. Jimenez, S. Ramanathan, P. Suraneni, W.J. Pestle, Use of thermogravimetric analysis to estimate collagen and hydroxyapatite contents in archaeological bone, J. Archaeol. Sci. 145 (2022) 105644.
[21] M. Gholipourmalekabadi, B. Farhadihosseinabadi, M. Faraji, M.R. Nourani, How preparation and preservation procedures affect the properties of amniotic membrane? how safe are the procedures? Burns 46 (2020) 1254–1271.
[22] R. Wang, C. Cheng, H. Wang, D. Wang, Swollen hydrogel nanotechnology: Advanced applications of the rudimentary swelling properties of hydrogels, ChemPhysMater 3 (2024) 357–375.
[23] F. Sahena, I.S.M. Zaidul, S. Jinap, A.A. Karim, K.A. Abbas, N.A.N. Norulaini, A.K. M. Omar, Application of supercritical CO2 in lipid extraction – a review, J. Food Eng. 95 (2009) 240–253.
[24] N.N. Giang, X.T. Trinh, J. Han, P.N. Chien, J. Lee, S.R. Noh, Y. Shin, S.Y. Nam, C. Y. Heo, Effective decellularization of human skin tissue for regenerative medicine by supercritical carbon dioxide technique, J. Tissue Eng. Regen. Med. 16 (2022) 1196–1207.
[25] P.M. Crapo, T.W. Gilbert, S.F. Badylak, An overview of tissue and whole organ decellularization processes, Biomaterials 32 (2011) 3233–3243.
[26] M. Rastgou-Maeini, A.Z. Hezave, S.H. Anjamrooz, F. Hosseinpour, A. Hassanpour-Dehnavi, Fabrication of testicular decellularized scaffolds using a hybrid SDS–supercritical CO_2 method: process optimization, extracellular matrix preservation, and biocompatibility evaluation, Biomed. Eng. Online 24 (2025) 143.
[27] J. Antons, M.G. Marascio, P. Aeberhard, G. Weissenberger, N. Hirt-Burri, L. A. Applegate, P.E. Bourban, D.P. Pioletti, Decellularised tissues obtained by a CO2-philic detergent and supercritical CO2, Eur. Cell. Mater. 36 (2018) 81–95.
[28] C. Gaudet, S. Odet, C. Meyer, B. Chatelain, E. Weber, A.L. Parmentier, S. Derruau, S. Laurence, C. Mauprivez, E. Brenet, H. Kerdjoudj, M. Fenelon, J.C. Fricain, N. Zwetyenga, D. Hoarau, R. Curien, E. Gerard, A. Louvrier, F. Gindraux, Reporting Criteria for Clinical Trials on Medication-Related Osteonecrosis of the Jaw (MRONJ): a Review and Recommendations, Cells 11 (2022) 4097.
[29] K. Belbachir, R. Noreen, G. Gouspillou, C. Petibois, Collagen types analysis and differentiation by FTIR spectroscopy, Anal. Bioanal. Chem. 395 (2009) 829–837.
[30] J. Hwang, B.H. San, N.J. Turner, L.J. White, D.M. Faulk, S.F. Badylak, Y. Li, S. M. Yu, Molecular assessment of collagen denaturation in decellularized tissues using a collagen hybridizing peptide, Acta Biomater. 53 (2017) 268–278.
[31] D. Gunasekaran, R. Thada, G.F.S. Jeyakumar, N.P. Manimegalai, G. Shanmugam, U.T. Sivagnanam, Physicochemical characterization and self-assembly of human

amniotic membrane and umbilical cord collagen: a comparative study, Int. J. Biol. Macromol. 165 (2020) 2920–2933.
[32] M.L. Tiffany, S. Krimm, Circular dichroism of the "random" polypeptide chain, Biopolymers 8 (1969) 347–359.
[33] C. Petibois, G. Gouspillou, K. Wehbe, J.P. Delage, G. Déleris, Analysis of type I and IV collagens by FT-IR spectroscopy and imaging for a molecular investigation of skeletal muscle connective tissue, Anal. Bioanal. Chem. 386 (2006) 1961–1966.
[34] R. Moseley, R. Waddington, P. Evans, B. Halliwell, G. Embery, The chemical modification of glycosaminoglycan structure by oxygen-derived species in vitro, Biochim. Biophys. Acta BBA - Gen. Subj. 1244 (1995) 245–252.
[35] A. Grémare, L. Thibes, M. Gluais, Y. Torres, D. Potard, N. Da Silva, N. Duserre, M. Fénelon, L. Sentilhes, S. Lacomme, I. Svahn, E. Gontier, J.C. Fricain, N. L'heureux, Development of a vascular substitute produced by weaving yarn made from human amniotic membrane, Biofabrication 14 (2022) ac84ae.
[36] C.S. Lau, A. Hassanbhai, F. Wen, D. Wang, N. Chanchareonsook, B.T. Goh, N. Yu, S. H. Teoh, Evaluation of decellularized tilapia skin as a tissue engineering scaffold, J. Tissue Eng. Regen. Med. 13 (2019) 1779–1791.
[37] C. Gaudet, L. Slolecki, B. Mathéaud, S. Odet, C. Meyer, A. Louvrier, F. Gindraux, Questions about Residual Cell Viability in Cryopreserved Human Amniotic Membrane and its Impact on Clinical applications, Biomedicines 10 (2022) 2456.
[38] K.H. Hussein, T. Saleh, E. Ahmed, H.H. Kwak, K.M. Park, S.R. Yang, B.J. Kang, K. Y. Choi, K.S. Kang, H.M. Woo, Biocompatibility and Hemocompatibility of Efficiently Decellularized whole Porcine Kidney for Tissue Engineering, J. Biomed. Mater. Res. A (2018) 2034–2047.
[39] H. Thomasen, M. Pauklin, K.P. Steuhl, D. Meller, Comparison of cryopreserved and air-dried human amniotic membrane for ophthalmologic applications, Graefes Arch. Clin. Exp. Ophthalmol. Albrecht Von Graefes Arch. Klin. Exp. Ophthalmol. 247 (2009) 1691–1700.
[40] R. Menezes, R. Vincent, L. Osorno, P. Hu, T.L. Arinzeh, Biomaterials and tissue engineering approaches using glycosaminoglycans for tissue repair: Lessons learned from the native extracellular matrix, Acta Biomater. 163 (2023) 210–227.
[41] A. Jiang, C. Li, Y. Gao, M. Zhang, J. Hu, W. Kuang, S. Hao, W. Yang, C. Xu, G. Gao, Z. Wang, Z. Liu, In vivo and in vitro inhibitory effect of amniotic extraction on neovascularization, Cornea 25 (2006) S36–S40.
[42] A. Wells, K. Gupta, P. Chang, S. Swindle, A. Glading, H. Shiraha, Epidermal growth factor receptor-mediated motility in fibroblasts, Microsc. Res. Tech. 43 (1998) 395–411.
[43] A. Jafari, M. Rezaei-Tavirani, H. Niknejad, H. Zali, Tumor Targeting by Conditioned Medium Derived from Human Amniotic Membrane: New Insight in Breast Cancer Therapy, Technol. Cancer Res. Treat. 20 (2021) 15330338211036318.
[44] J.B. Baudey, L. Solecki, C. Picard, P. Pedini, B. Mathéaud, A. Coaquette, I. Jollet, P. Jamain, L. Hubert, A. Desanlis, X. Lafarge, F. Gindraux, Reassessing the cryopreserved human amniotic membrane's low immunogenicity due to advances in histocompatibility, Mater. Today Bio 35 (2025) 102619.
[45] H. Rammal, C. Bour, M. Dubus, L. Entz, L. Aubert, S.C. Gangloff, S. Audonnet, N. B. Bercu, F. Boulmedais, C. Mauprivez, H. Kerdjoudj, Combining Calcium Phosphates with Polysaccharides: a Bone-inspired Material Modulating Monocyte/Macrophage Early Inflammatory Response, Int. J. Mol. Sci. 19 (2018) 113458.
[46] A. Navas, F.S. Magaña-Guerrero, A. Domínguez-López, C. Chávez-García, G. Partido, E.O. Graue-Hernández, F.J. Sánchez-García, Y. Garfias, Anti-Inflammatory and Anti-Fibrotic Effects of Human Amniotic Membrane Mesenchymal Stem Cells and their potential in Corneal Repair, Stem Cells Transl. Med. 7 (2018) 906–917.
[47] M. Topka, Y. Zhang, A. Bock, P. Riedel, J. Lörner, A. Hammer, E. Maier, F. Paulsen, C.M. Hammer, Usability of abattoir-acquired pig eyes for refractive excimer laser research, Sci. Rep. 11 (2021) 19087.